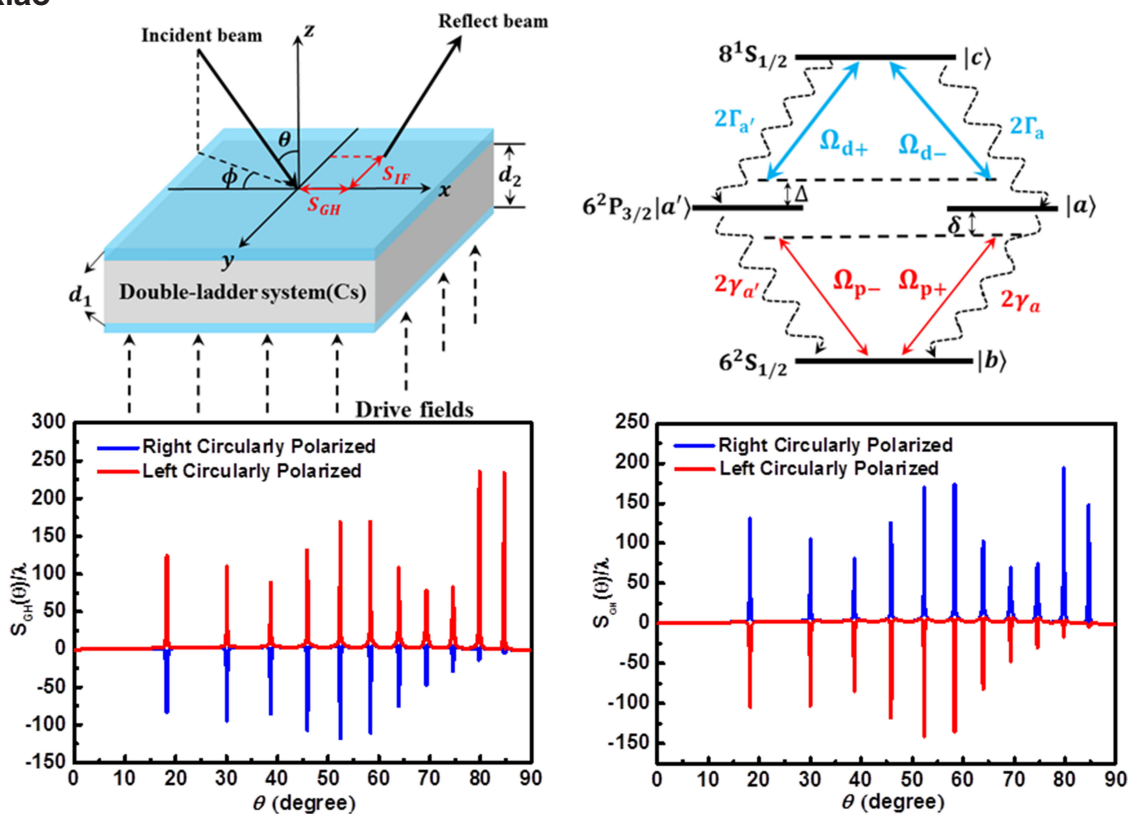


Tunable Goos–Hänchen Shift and Polarization Beam Splitting Through a Cavity Containing Double Ladder Energy Level System



Volume 11, Number 2, April 2019

Peng Han
Xiaoyang Chang
Wenxiu Li
Hao Zhang
Anping Huang
Zhisong Xiao



DOI: 10.1109/JPHOT.2019.2897280
1943-0655 © 2019 IEEE

Tunable Goos–Hänchen Shift and Polarization Beam Splitting Through a Cavity Containing Double Ladder Energy Level System

Peng Han ¹, Xiaoyang Chang,¹ Wenxiu Li,¹ Hao Zhang ²,
Anping Huang,¹ and Zhisong Xiao ^{1,3}

¹Key Laboratory of Micro-nano Measurement, Manipulation and Physics (Ministry of Education), School of Physics and Nuclear Energy Engineering, Beihang University, Beijing 100191, China

²Frontier Research Institute of Innovative Science and Technology, Beihang University, Beijing 100191, China

³Beijing Academy of Quantum Information Sciences, Beijing 100193, China

DOI:10.1109/JPHOT.2019.2897280

1943-0655 © 2019 IEEE. Translations and content mining are permitted for academic research only. Personal use is also permitted, but republication/redistribution requires IEEE permission. See http://www.ieee.org/publications_standards/publications/rights/index.html for more information.

Manuscript received November 17, 2018; revised December 28, 2018; accepted January 29, 2019. Date of publication February 21, 2019; date of current version March 5, 2019. This work was supported in part by the International S&T Cooperation Program of China under Grant 2014DFA52000, in part by the Beijing Academy of Quantum Information Sciences under Grant Y18G28, and in part by the National Natural Science Foundation of China under Grant 11574021, Grant 11574017, Grant 51372008, and Grant 11804017. Corresponding author: Zhisong Xiao (e-mail: zsxiao@buaa.edu.cn).

Abstract: The present paper theoretically demonstrates tunable Goos–Hänchen (GH) shift and beam splitting of the polarized light reflected from the cavity containing the double ladder energy level system. Simultaneously opposite GH shifts for left-circularly polarized (LCP) and right-circularly polarized (RCP) beams can be achieved under asymmetric field conditions. By adjusting the intensity (Rabi frequency) of probe or drive field, the GH shifts of LCP and RCP probe beams are manipulated at the same time. We also discuss the effects of probe field frequency detuning on GH shifts and identify the parameters region to obtain a large separate distance ($\sim 320 \mu\text{m}$) between LCP and RCP probe beams.

Index Terms: Goos–Hänchen shift, Double ladder energy level system, Beam splitting.

1. Introduction

When a light beam is incident on the interface of two different dielectric media, the centroid of totally reflected light beam undergoes a longitude shift that deviated from the position predicted by geometrical reflection. This interesting phenomenon was known as Goos–Hänchen (GH) effect which has been experimentally verified by Goos and Hänchen in 1947 and the longitude shift was called GH shift [1]. The GH effect was theoretically explained by stationary phase method and energy flux method [2]–[3]. On the basis of these pioneer works, the GH effect was extensively investigated due to its potential applications in various fields involving optical sensors [4]–[7], acoustics [8], plasma physics [9]–[10] and quantum mechanics [11]–[13].

In general, the magnitude of the reflected GH shift is only several times of wavelengths, which is rather difficult to be observed and measured in the experiment. Various structures and materials

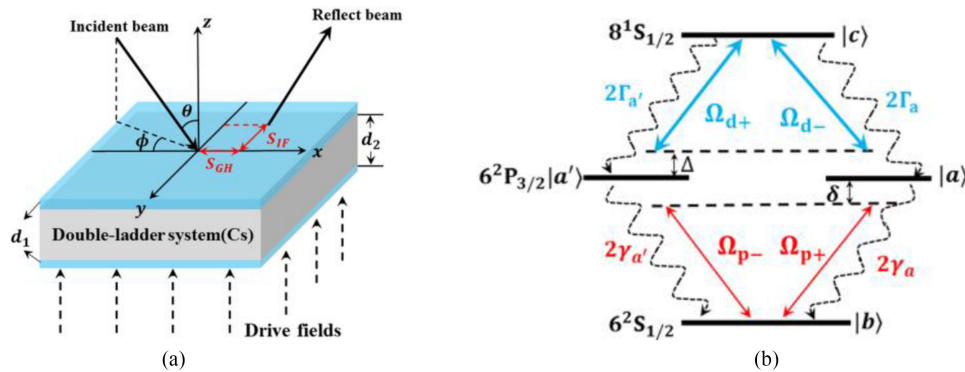


Fig. 1. (a) Schematic of a weak probe beam incident upon the cavity containing double ladder energy level system, the probe beam is reflected back with a longitudinal shift (SGH) and a transverse shift (SIF). (b) Energy level structure of the intracavity medium.

were studied to enhance the magnitude of the GH shift [14]–[17]. Large positive GH shifts can be obtained through multilayered and periodic structures [18]–[20], waveguide structures [21]–[22] and artificial materials [23]–[25]. Moreover, negative GH shifts were demonstrated when the light beam was reflected from slab configurations containing absorptive dielectric medium [26]–[27] and left-handed materials [28]. It is noticeable that the GH shifts also depend on the polarization state of the light beam since the reflection coefficient is different for TE and TM polarized beams under same conditions [27]–[30]. Simultaneously opposite GH shifts for reflected TE and TM polarized beams were proved in theory and experiments by using asymmetric double-prism configuration, metal-cladding waveguide and single negative materials [30]–[32]. The beam splitting based on opposite GH shifts cannot be controlled in a fixed configuration which is inconvenient for a tunable optical device.

Besides elevating the magnitude of the GH shift, modulation of the GH shift in a large range is another significant development. Without changing the structure of the configuration, various medium (for example: atom gas, quantum well and carbon nanotube quantum dot) with different energy level structures were injected into a cavity to manipulate the GH shifts by only adjusting external parameters [33]–[45]. Due to the modification of the absorption-dispersion relation of the intracavity medium using coherent driving field, the GH shifts were controlled through a cavity containing a two-level atomic system [33]. Afterwards, Ziauddin et al. reported control of the GH shift for the beam reflected from the cavity containing three- and four-level atomic medium [34]. The reflected positive and negative GH shifts correspond to subluminal and superluminal propagation of the probe beam respectively [34]. Simultaneously positive and negative GH shifts in reflected and transmitted beams were achieved due to the Rydberg state of the intracavity medium [45]. However, controllable and concurrently opposite GH shifts in only the reflected beams is not reported in such a cavity configuration, the related application is undeveloped as well.

In this paper, large and tunable positive and negative GH shifts can be simultaneously achieved through the cavity containing a double ladder energy level system. The emergence of such phenomenon is due to the realization of concurrently subluminal and superluminal propagation in intracavity medium. The behavior of GH shifts for reflected LCP and RCP beams are easily manipulated at the same time via adjusting probe or drive field. The distance of the beam splitting can be upgraded to hundreds of micrometers.

2. Model and Atomic Dynamics

As depicted in Fig. 1a, the cavity configuration contains a double ladder energy level system ($\epsilon_2 = 1 + \chi$) bounded by two identical nonmagnetic dielectric slabs (ϵ_1). The thickness of the slab and the atomic medium is d_1 and d_2 respectively. The probe beam E_p with angular frequency ω_p

incident from vacuum ($\varepsilon_0 = 1$) upon the cavity at an incident angle θ and is reflected back with a longitude shift (S_{GH}). The transverse shift corresponds to the Imbert–Fedorov shift (S_{IF}) which has been widely investigated in previous works [47]–[49]. Generally, the reflection coefficient $r_{TE/TM}$ of the cavity can be obtained through transfer matrix approach. For the j -th layer, the transfer matrix is

$$M_j(k_y, \omega_p, d_j) = \begin{pmatrix} \cos[k_z^j d_j] & i \sin[k_z^j d_j] / q_j \\ i q_j \sin[k_z^j d_j] & \cos[k_z^j d_j] \end{pmatrix} \quad (1)$$

where $k_z^j = \sqrt{\varepsilon_j k^2 - k^2 \sin^2 \theta}$ is the z component of the wave number in j -th layer, $k = \omega_p / c$ is the wave number and the c is the speed of light in vacuum, $q_j = \sqrt{\varepsilon_j - \sin^2 \theta}$ is TE polarized beam and $q_j = \frac{1}{\varepsilon_j} \sqrt{\varepsilon_j - \sin^2 \theta}$ is TM polarized beam in j -th layer [27], [33]. The total transfer matrix can be expressed as

$$Q(k_y, \omega_p) = M_1(k_y, \omega_p, d_1) M_2(k_y, \omega_p, d_2) M_3(k_y, \omega_p, d_1). \quad (2)$$

The reflection coefficients $r_{TE/TM}$ is given by

$$r_{TE/TM}(\theta) = \frac{\cos \theta (Q_{22} - Q_{11}) - (\cos^2 \theta Q_{12} - Q_{21})}{\cos \theta (Q_{22} + Q_{11}) - (\cos^2 \theta Q_{12} + Q_{21})} \quad (3)$$

Q_{ij} is the elements of the total matrix $Q(k_y, \omega_p)$ [33]–[34]. In order to modify the reflection coefficient of the cavity, it is necessary to analyze the dielectric function of the double ladder energy level system.

The energy level structure could be realized using cesium atoms [46], [50], [51]. As Fig. 1b shown, it contains a ground state level $|b\rangle(6^2S_{1/2})$ and an excited state level $|c\rangle(8^1S_{1/2})$, the intermediate states $|a\rangle$ and $|a'\rangle(6^2P_{3/2})$ are degenerate Zeeman states with $m_j = \pm 1$. For a linearly polarized probe beam E_p , the LCP(σ^-) and RCP(σ^+) components have the same frequency and they simultaneously couple the transitions $|b\rangle \leftrightarrow |a'\rangle$ and $|b\rangle \leftrightarrow |a\rangle$ [50]–[52], Ω_{p-} and Ω_{p+} are the Rabi frequencies of the probe fields. The strong driving fields with Rabi frequencies Ω_{d-} and Ω_{d+} are vertically incident on the cavity and couple the transitions $|a\rangle \leftrightarrow |c\rangle$ and $|a'\rangle \leftrightarrow |c\rangle$ homogeneously as shown in Fig. 1, the frequency detuning of the probe and drive field are δ and Δ respectively. The decay rates of the transition $|c\rangle \rightarrow |a\rangle$, $|a'\rangle$ and $|a\rangle, |a'\rangle \rightarrow |b\rangle$ are $2\Gamma_{a,a'}$ and $2\gamma_{a,a'}$.

In the interaction picture, under rotating wave and electric dipole approximation, the total Hamiltonian of the atomic system is

$$H = H_0 + H_I \quad (4)$$

where the free Hamiltonian H_0 and the interaction Hamiltonian H_I are expressed as

$$H_0 = \hbar (\omega_a |a\rangle \langle a| + \omega_{a'} |a'\rangle \langle a'| + \omega_c |c\rangle \langle c|) \quad (5)$$

$$H_I = -\hbar [(\Omega_{d+} |c\rangle \langle a| + \Omega_{d-} |c\rangle \langle a'|) e^{-i\omega_d t} + (\Omega_{p+} |a\rangle \langle b| + \Omega_{p-} |a'\rangle \langle b|) e^{-i\omega_p t} + H.c.] \quad (6)$$

ω_p and ω_d are the frequencies of the probe and drive fields respectively. The atomic dynamic equation of the atomic medium is given by the density matrix equation

$$\frac{\partial \rho}{\partial t} = -\frac{i}{\hbar} [H_0 + H_I, \rho] - \sum_{i=a,a'} (\Gamma_i \{ |c\rangle \langle c|, \rho \}_+ + \gamma_i \{ |i\rangle \langle i|, \rho \}_+ - 2\Gamma_i \rho_{cc} |i\rangle \langle i| - 2\gamma_i \rho_{cc} |b\rangle \langle b|) \quad (7)$$

here $\{ \}_+$ is the anticommutators of the operators. For simplicity, we assume the Rabi frequencies $|\Omega_{d\pm}|^2 \gg |\Omega_{p\pm}|^2$ and the decay rates $2\Gamma = 2\Gamma_i (i = a, a')$, $2\gamma = 2\gamma_i (i = a, a')$ [50], [51]. According to the relation $P_{\pm} = N \wp \rho_{\pm}$, the susceptibilities χ_{\pm} for LCP and RCP probe beams are given by

$$\chi_{\pm} = \frac{i\eta}{\Omega_{p\pm} D} [\Omega_{p\pm} (|\Omega_{d\pm}|^2 + (\gamma + i\delta) (2\Gamma + i(\Delta + \delta))) - \Omega_{p\mp} \Omega_{d\mp}^* \Omega_{d\pm}] \quad (8)$$

$$D = (\gamma + i\delta) [|\Omega_{d+}|^2 + |\Omega_{d-}|^2 + (\gamma + i\delta) (2\Gamma + i(\Delta + \delta))]$$

where η is $N\varphi^2/\hbar\varepsilon$, P is the atomic polarization, N is the number density of atom vapor and φ represents the dipole moment of the transition $|b\rangle \leftrightarrow |a\rangle(|a'\rangle)$. Here, $\chi_{\pm} = \text{Re}(\chi_{\pm}) + i \cdot \text{Im}(\chi_{\pm})$, the real part $\text{Re}(\chi_{\pm})$ is corresponding to the dispersion while the imaginary part $\text{Im}(\chi_{\pm})$ is corresponding to the gain or loss. The dispersion behavior of the whole configuration depends on the intracavity medium and the nonmagnetic slabs [34]. Group index of the cavity N_g^r are expressed as

$$N_g^r = \frac{c}{v_g^r} = \frac{c}{L} \frac{\partial \varphi_r}{\partial \omega_p} \quad (9)$$

$L = 2d_1 + d_2$ denotes the thickness of the whole configuration. It can be seen from Eq. (9) the group index of the configuration depends on the thickness of the whole configuration and the derivative of the reflected probe beams phase φ_r with respect to the probe light field frequency ω_p .

The expressions for reflected GH shift are achieved based on numerical simulation and stationary phase theory. As Fig. 1a demonstrated, on the plane $z = 0$, the GH shift is defined as $\langle x_r \rangle - \langle x_i \rangle$, $\langle x_i \rangle$ and $\langle x_r \rangle$ represents the x coordinates of the centroid of incident and reflected beams respectively [42], [53], [54]. A well-collimated monochromatic beam with spatial Gaussian profile is considered to incident on the cavity configuration. The vector electric field $\mathbf{E}_{i/r}(r)$ of incident and reflected beams can be written in terms of their vector angular spectrum [42], [53]

$$\mathbf{E}_{i/r}(r) = \frac{1}{2\pi} \iint \mathbf{A}_{i/r}(k_x, k_y) \exp(i\mathbf{k} \cdot \mathbf{r}) dk_x dk_y \quad (10)$$

where $\mathbf{A}_{i/r}(k_x, k_y) = (\mathbf{A}_{i/rx}, \mathbf{A}_{i/ry}, \mathbf{A}_{i/rz})^T$ refers to the vector amplitude of the angular spectrum, k_x and k_y is the x and y component of the wave number k , T means transpose. For an arbitrarily polarized incident beam, the electric fields of the light beams are divided into TE and TM polarized components for calculation, the vector angular spectrum are

$$\mathbf{A}_i(k_x, k_y) = c_{TE} \begin{pmatrix} \sin \phi \\ -\cos \phi \\ 0 \end{pmatrix} A_G + c_{TM} \begin{pmatrix} -\cos \theta \cos \phi \\ -\cos \theta \sin \phi \\ \sin \theta \end{pmatrix} A_G \quad (11)$$

$$\mathbf{A}_r(k_x, k_y) = c_{TE} \cdot r_{TE}(\theta) \begin{pmatrix} \sin \phi \\ -\cos \phi \\ 0 \end{pmatrix} A_G + c_{TM} \cdot r_{TM}(\theta) \begin{pmatrix} \cos \theta \cos \phi \\ \cos \theta \sin \phi \\ \sin \theta \end{pmatrix} A_G \quad (12)$$

c_{TE} and c_{TM} give a description of polarization state of the beam and satisfy the normalization condition $|c_{TE}|^2 + |c_{TM}|^2 = 1$ [42], [53]. For linearly polarized light, $c_{TE} = 1$ and $c_{TM} = 0$. While for circularly polarized light beam, $c_{TE} = 1/\sqrt{2}$ and $c_{TM} = i/\sqrt{2}$ correspond to the LCP component, $c_{TE} = 1/\sqrt{2}$ and $c_{TM} = -i/\sqrt{2}$ correspond to the RCP component [42]. The Gaussian function defined the spatial profile of the incident light beam is represented by

$$A_G = \sqrt{\frac{W_x W_y}{\pi}} \exp\left[-\frac{W_x^2(k_x - k_{x0})^2}{2}\right] \exp\left[-\frac{W_y^2(k_y - k_{y0})^2}{2}\right] \quad (13)$$

where $W_x = W/\cos \theta$, $W_y = W$, W is the half-width of the beam waist, the initial angular spectrum distribution is considered to be sharply distributed around the principle axis $(k_{x0}, k_{y0}) = (k \sin \theta, 0)$ [42], [53]. The x coordinates of the centroid of the incident and reflected beams are

$$\langle x_{i/r} \rangle = \frac{\iint \psi_{i/r}^* \cdot x \cdot \psi_{i/r} dx dy}{\iint \psi_{i/r}^* \cdot \psi_{i/r} dx dy} \quad (14)$$

$\psi_{i/r}$ is the vector electric field on the plane $z = 0$. For an incident probe beam with sufficiently large width (*i.e.*, narrow angular spectrum), according to the stationary phase theory, the GH shift of the reflected beam also can be estimated as $S_{GH}^{TE/TM} = -(\lambda/2\pi)(d\varphi_r^{TE/TM}/d\theta)$ [42], [54], $\varphi_r^{TE/TM}$ is the phase of the reflection coefficient $r_{TE/TM}(\theta)$. The expression of the reflected GH shift is obtained by

summing the weighted contributions of TE and TM polarized components

$$\langle x_r \rangle - \langle x_i \rangle \approx S_{GH} = \frac{|c_{TE} r^{TE}(\theta)|^2 S_{GH}^{TE} + |c_{TM} r^{TM}(\theta)|^2 S_{GH}^{TM}}{|c_{TE} r^{TE}(\theta)|^2 + |c_{TM} r^{TM}(\theta)|^2} \quad (15)$$

here, S_{GH}^{TE} and S_{GH}^{TM} represent the GH shifts of TE and TM polarized components respectively [42], [53], [54]. The approximation in Eq. (15) is valid when the reflected beam is not greatly distorted [42], [54].

3. Results and Discussions

In this section, we analyze the behavior of the GH shift for reflected probe beam, both of the symmetric and asymmetric cases of the double ladder energy level system are discussed. Parameters including the drive fields intensities, probe fields intensities and probe field frequency detuning are employed to adjust the susceptibilities of atomic medium, thus, the reflected GH shifts are controlled.

In the following, we set $d_1 = 0.1 \mu\text{m}$, $d_2 = 5 \mu\text{m}$, $\varepsilon_1 = 2.22$ throughout this paper unless specified. The probe fields are assumed to be resonant with the transition $6^2S_{1/2} \leftrightarrow 6^2P_{3/2}$ at wavelength 852.2nm, while the drive fields are resonant with the transition $6^2P_{3/2} \leftrightarrow 8^1S_{1/2}$ at wavelength 794.3nm [51], [55]. The decay rates from $8^1S_{1/2} \rightarrow 6^2P_{3/2}$ and from $6^2P_{3/2} \rightarrow 6^2S_{1/2}$ is $2\pi \times 1.7 \text{ MHz}$ and $2\pi \times 5.2 \text{ MHz}$ respectively [51], [55].

All of the probe fields and drive fields are set to be nonzero, dual ladder electromagnetically-induced-transparency (EIT) configuration of the double ladder energy level is established, which can be interpreted by the creation of dark state between $|b\rangle$ and $|c\rangle$ as shown in Fig. 1b [51]. The dark state created by probe field Ω_{p+} and drive field Ω_{d-} is perturbed owing to the presence of drive field Ω_{d+} , which further increases the absorption of the probe field Ω_{p+} . The population is pumped to the excited state $|c\rangle$ via the drive field Ω_{d-} , transferred to the state $|a\rangle$ owing to the stimulated emission via the drive field Ω_{d+} [51]. Thus, gain is achieved in the probe field Ω_{p-} due to the three photon process $\Omega_{d+}^* \Omega_{d-} \Omega_{p+}$ via the transition $|b\rangle \rightarrow |a\rangle \rightarrow |c\rangle \rightarrow |a'\rangle$. Meanwhile, the dark state created by probe field Ω_{p-} and drive field Ω_{d+} is also perturbed by the drive field Ω_{d-} , similar three photon process $\Omega_{d-}^* \Omega_{d+} \Omega_{p-}$ occurs through the transition $|b\rangle \rightarrow |a'\rangle \rightarrow |c\rangle \rightarrow |a\rangle$. In a word, gain and loss properties of the probe beams are tunable, determined by the combination of the ladder-EIT and the three photon process [46].

3.1 Symmetric Case

We first discuss the symmetric case of the double ladder energy level system *i.e.*, $\Omega_{p+} = \Omega_{p-}$, $\Omega_{d+} = \Omega_{d-}$. In Fig. 2a and Fig. 2b, the absorption and dispersion behavior of the probe beams are plotted as a function of the probe field detuning δ with $\Omega_{p\pm} = 0.1\gamma$, $\Omega_{d\pm} = 5\gamma$. The ladder-EIT configuration created via Ω_{p+}/Ω_{d-} is equivalent with that created via Ω_{p-}/Ω_{d+} . Moreover, the three-photon process $\Omega_{d-}^* \Omega_{d+} \Omega_{p-}$ and $\Omega_{d+}^* \Omega_{d-} \Omega_{p+}$ are the same, the energy transfer via $|b\rangle \rightarrow |a'\rangle \rightarrow |c\rangle \rightarrow |a\rangle$ and $|b\rangle \rightarrow |a\rangle \rightarrow |c\rangle \rightarrow |a'\rangle$ are equal. Thus, the absorption and dispersion behavior of the two probe beams are identical *i.e.*, $\chi_+ = \chi_-$.

In Fig. 2c, the behavior of GH shifts for reflected LCP and RCP probe beams are plotted as a function of the incident angles θ based on Eq. (15) with $\delta = 0$. The GH shifts are enhanced in negative direction when the resonant conditions of the cavity are satisfied. The curves of GH shifts for the two probe beams are coincide with each other, the GH shifts behavior of reflected LCP and RCP probe beams are identical. Fig. 2d demonstrates the reflection model for symmetric case of the atomic medium, a linearly polarized light beam is incident on the cavity and reflected with negative GH shifts when the resonant conditions of the cavity are satisfied. It can be seen from Fig. 2c and Fig. 2d that beam splitting based on simultaneously opposite GH shifts for LCP and RCP probe beams cannot be achieved in symmetric case of the double ladder energy level system.

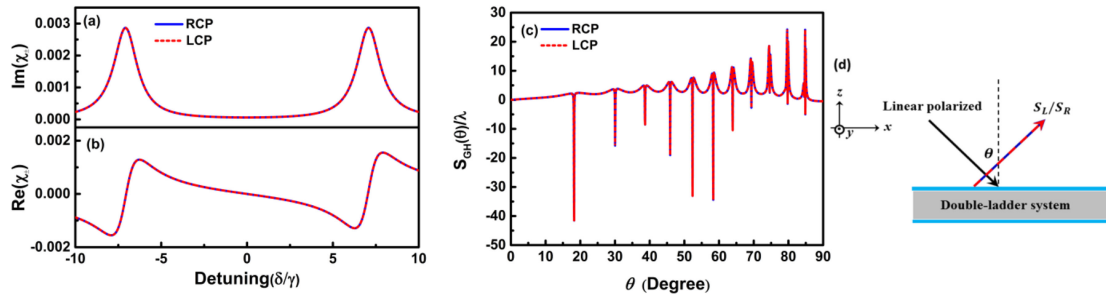


Fig. 2. (a)-(b) Dependence of the imaginary $\text{Im}(\chi_{\pm})$ and real $\text{Re}(\chi_{\pm})$ susceptibilities on probe detuning δ for symmetric case. (c) The GH shifts of the probe beams as a function of the incident angles θ for symmetric case with $\delta = 0$. In all of the figures, the red dashed and black solid lines correspond to the LCP and RCP probe beams. The selected parameters are $N = 1 \times 10^{11}/\text{cm}^3$, $\delta\rho = 2.685 \times 10^{-29}$ C·m, the intensities of the drive and probe fields are $\Omega_{d\pm} = 5\gamma$, $\Omega_{p\pm} = 0.1\gamma$. (d) The reflection model of the symmetric case.

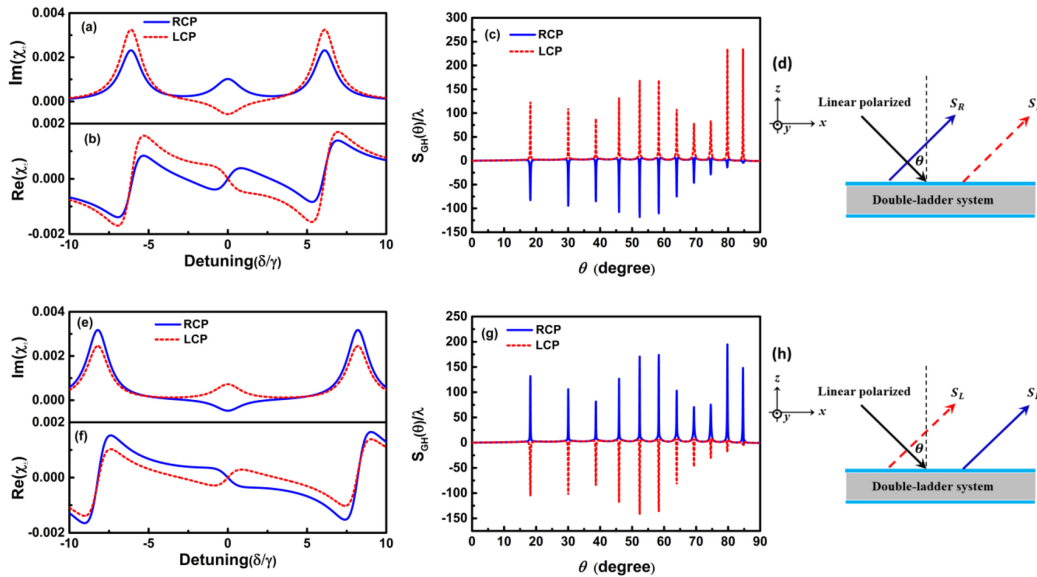


Fig. 3. (a)-(b), (e)-(f): Dependence of the susceptibilities on probe detuning δ for drive asymmetric cases. (c), (g): The GH shifts of the probe beams as a function of the incident angles θ for drive asymmetric cases with $\delta = 0$. (d), (h): the reflection model for drive asymmetric cases. In all of the figures, the red dashed and black solid lines correspond to the LCP and RCP probe beams. Here, $\Omega_{p+} = \Omega_{p-} = 0.1\gamma$, $\Omega_{d+} = 5\gamma$, for (a)-(d) $\Omega_{d-} = 3.5\gamma$, for (e)-(h) $\Omega_{d-} = 6.5\gamma$, other parameters are the same as in Fig. 2.

3.2 Asymmetric Case

In this section, we discuss the asymmetric case of the double-ladder energy level system, including the case of drive field asymmetry ($\Omega_{p+} = \Omega_{p-}$, $\Omega_{d+} \neq \Omega_{d-}$) and probe field asymmetry ($\Omega_{d+} = \Omega_{d-}$, $\Omega_{p+} \neq \Omega_{p-}$). In Fig. 3a, the imaginary parts of the susceptibilities are plotted as a function of the probe field detuning δ with $\Omega_{p\pm} = 0.1\gamma$, $\Omega_{d+} = 5\gamma$ and $\Omega_{d-} = 3.5\gamma$. As $\Omega_{d+} > \Omega_{d-}$, the combination of ladder-EIT and three-photon process $\Omega_{d+}^* \Omega_{d-} \Omega_{p+}$ lead to net gain for LCP probe beam that is associated with loss of RCP probe beam (in the region $\delta \sim 0$). In Fig. 3b, on the basis of Kramers-Kronig relation, the coexistence of gain and loss implies that normal and anomalous dispersion could be simultaneously generated for the two probe beams in the region $\delta \sim 0$. Therefore, concurrently subluminal and superluminal wave propagation are realized in the intracavity medium. Fig. 3c demonstrates the behavior of the GH shifts as a function of the incident angles θ , large positive

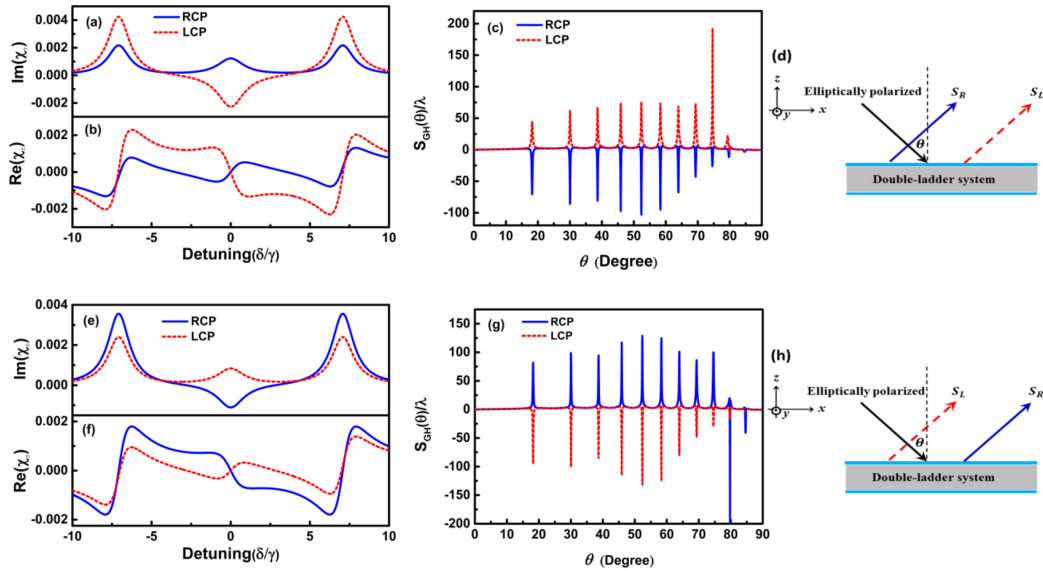


Fig. 4. (a)-(b), (e)-(f): Dependence of the susceptibilities on probe detuning δ for probe asymmetric cases. (c), (g): The GH shifts of the probe beams as a function of the incident angles θ for probe asymmetric cases with $\delta = 0$. (d), (h): the reflection model for probe asymmetric cases. In all of the figures, the red dashed and black solid lines correspond to the LCP and RCP probe beams. Here, $\Omega_{d+} = \Omega_{d-} = 5\gamma$, $\Omega_{p+} = 0.1\gamma$, for (a)-(d) $\Omega_{p-} = 0.05\gamma$, for (e)-(h) $\Omega_{p-} = 0.15\gamma$, other parameters are the same as in Fig. 2.

and negative GH shifts are simultaneously achieved when the resonant condition of the cavity are satisfied. The GH shift of the LCP and RCP beam is positive and negative respectively. As depicted in Fig. 3d, a linearly polarized probe beam is incident on the cavity, the LCP and RCP beams are reflected with opposite GH shifts at the same time. In Fig. 3a–Fig. 3d, positive and negative GH shifts correspond to the subluminal and superluminal propagation of the probe beams respectively. The physical mechanism of the result can be explained through the group index of the configuration. According to the Eq. (9), the group index of the reflected probe beams is positive (negative) whenever the GH shifts is positive (negative) [34].

The intensity of the drive field Ω_{d-} is adjusted from 3.5γ to 6.5γ , keeping the rest of the parameters unchanged. Compared with the case in Fig. 3a, gain and loss properties of the probe beams are modified when the intensity of Ω_{d-} is larger than Ω_{d+} , the LCP beam experiences loss, while the RCP beam experiences gain in the region $\delta \sim 0$ as shown in Fig. 3e. Both normal and anomalous dispersion of the probe beams reappear simultaneously as shown in Fig. 3f, opposite to the case in Fig. 3b. As Fig. 3g demonstrated, the GH shift of LCP probe beam is negative and the RCP probe beam suffers positive GH shift, the corresponding model is depicted in Fig. 3h. By only manipulating the intensity of drive field to control the absorption-dispersion relations, the GH shift can be switched from positive (negative) to negative (positive) for orthogonal circularly polarized light beams in such a fixed cavity configuration.

Next, we turn to discuss the case of probe asymmetry, the incident light beam is elliptically polarized. Probe absorption and dispersion curves for reflected probe beams are plotted in Fig. 4a and Fig. 4b. In the region $\delta \sim 0$, net gain is achieved in LCP probe field Ω_{p-} owing to the absorption of Ω_{p+} through the three-photon process $\Omega_{d+}^* \Omega_{d-} \Omega_{p+}$. The GH shift of LCP beam is positive owing to the subluminal wave propagation, while the RCP beam suffers negative GH shift owing to the superluminal wave propagation as shown in Fig. 4c. The result is similar to the case shown in Fig. 3c.

In Fig. 4e–Fig. 4g, the intensity of Ω_{p-} is adjusted from 0.05γ to 0.15γ while maintaining the other parameters unchanged, the susceptibilities demonstrate similar characteristics with the case

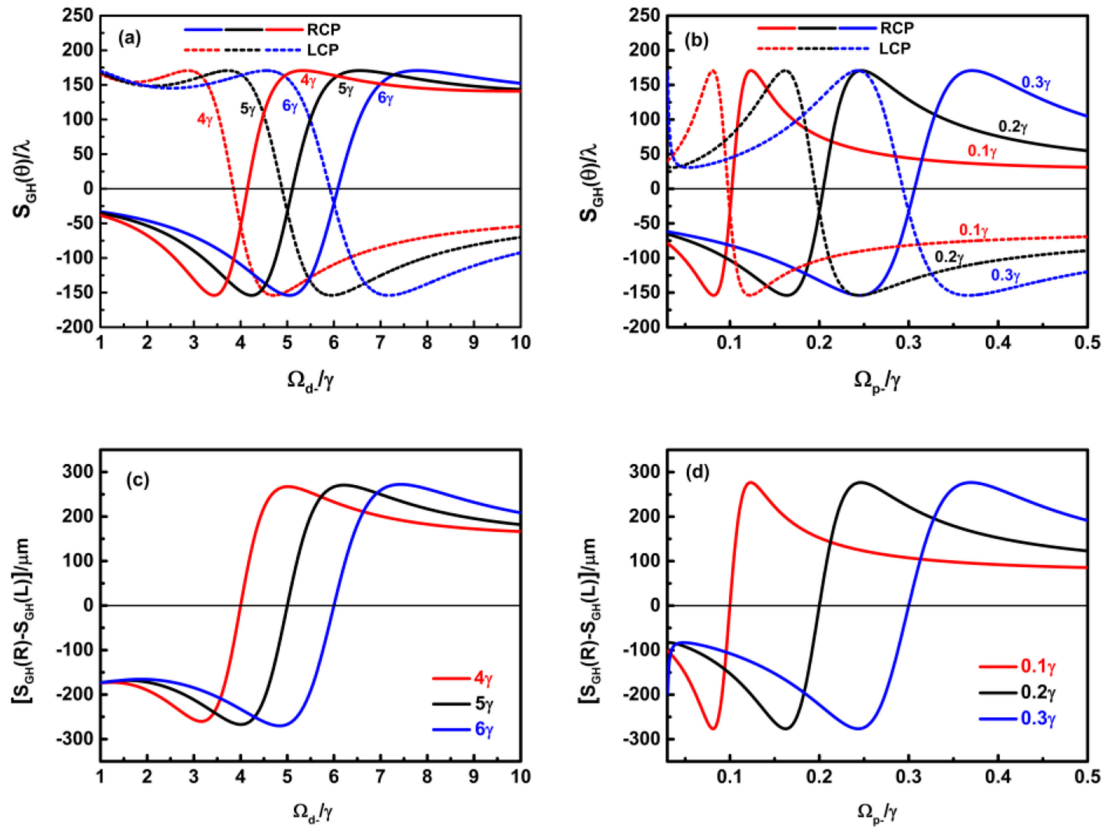


Fig. 5. (a). The behavior of GH shifts versus the intensities of drive fields Ω_{d-} with different values of Ω_{d+} : red line – 4γ , black line – 5γ , blue line – 6γ , $\Omega_{p+} = \Omega_{p-} = 0.1\gamma$. (b). The behavior of GH shifts versus the intensities of probe fields Ω_{p-} with different values of Ω_{p+} : red line – 0.1γ , black line – 0.2γ , blue line – 0.3γ , $\Omega_{d+} = \Omega_{d-} = 5\gamma$. The incident angle is $\theta = 52.37^\circ$, other parameters are same as in Fig. 2. (c)–(d), separate distance $[S_{GH}(R) - S_{GH}(L)]/\mu\text{m}$ versus (c). drive fields with red line – 4γ , black line – 5γ , blue line – 6γ and (d). probe fields with red line – 0.1γ , black line – 0.2γ , blue line – 0.3γ .

shown in Fig. 3e–Fig. 3f, LCP and RCP beams experience gain and loss respectively. The behavior of GH shifts are plotted in Fig. 4g, compared with the case in Fig. 4c, the GH shift of the LCP beam is switched from positive to negative, while the GH shift of RCP beam is switched from negative to positive at the same time. Fig. 4d and 4h shows the reflection model for probe asymmetric case of the atomic medium. These results indicate that the behavior of the GH shifts also can be tuned by adjusting the intensity of the probe field.

3.3 Dependence of the GH Shifts on Drive and Probe Field Intensities

Based on the above discussions, it is worthwhile to study the dependence of GH shifts on intensities of the probe and drive fields. Fig. 5a demonstrates the GH shifts as a function of the intensities of the drive fields (Ω_{d-}) with different Ω_{d+} . The GH shifts versus the intensities of the probe fields (Ω_{p-}) with different Ω_{p+} are depicted in Fig. 5b. The incident angle is fixed at $\theta = 52.37^\circ$ when a large separate distance between LCP and RCP probe beams could be achieved based on Fig. 3 and Fig. 4. The probe field detuning is fixed at $\delta = 0$.

For RCP probe beam, with increase of the intensities of drive (Ω_{d-}) or probe fields (Ω_{p-}), the GH shift is enhanced to the maximal values in negative direction, decreased to 0 and switched from negative to positive at the critical points [Fig. 5a: $4\gamma \rightarrow 4.15\gamma$, $5\gamma \rightarrow 5.11\gamma$, $6\gamma \rightarrow 6.07\gamma$, Fig. 5b:

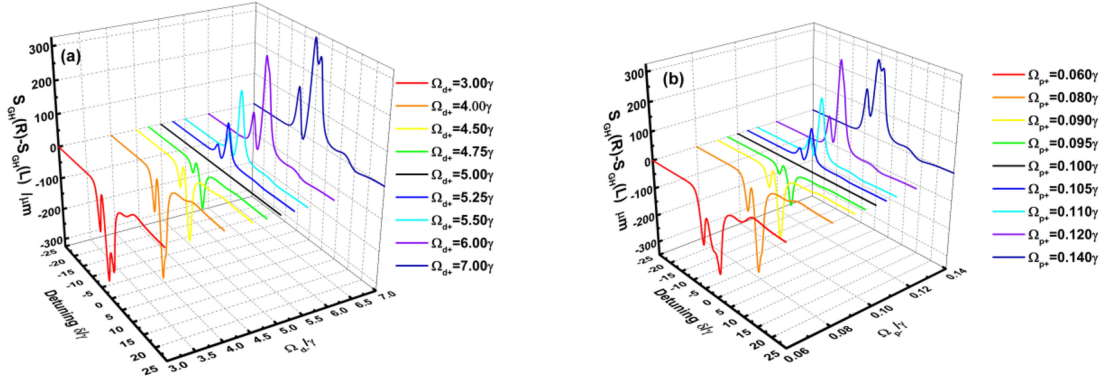


Fig. 6. The dependence of the GH shifts as a function of the probe detuning δ at incident angle $\theta = 52.37^\circ$ with (a). different intensities of drive fields Ω_{d-} ranging from 3γ to 7γ , the selected parameters are: $\Omega_{p+} = \Omega_{p-} = 0.1\gamma$, $\Omega_{d+} = 5\gamma$ (b) different intensities of probe fields Ω_{p-} ranging from 0.06γ to 0.14γ , the selected parameters are: $\Omega_{d+} = \Omega_{d-} = 5\gamma$, $\Omega_{p+} = 0.1\gamma$.

$0.1\gamma \rightarrow 0.102\gamma$, $0.2\gamma \rightarrow 0.204\gamma$, $0.3\gamma \rightarrow 0.307\gamma$], reaches towards the peak value in positive direction as shown in Fig. 5a and Fig. 5b. For LCP probe beam, with the increase of the intensities of drive (Ω_{d-}) or probe fields (Ω_{p-}), the GH shift is enhanced in positive direction, decreased from the maximal value to 0 and switched to negative direction at critical point [Fig. 5a: $4\gamma \rightarrow 3.82\gamma$, $5\gamma \rightarrow 4.87\gamma$, $6\gamma \rightarrow 5.91\gamma$, Fig. 5b: $0.1\gamma \rightarrow 0.097\gamma$, $0.2\gamma \rightarrow 0.195\gamma$, $0.3\gamma \rightarrow 0.294\gamma$], promoted to the peak value in negative direction. As depicted in Fig. 5a and Fig. 5b, the behavior of GH shifts for LCP and RCP beams are manipulated at the same time by adjusting the intensities of the applied fields. Opposite GH shifts are simultaneously achieved for LCP and RCP beams with $\Omega_{d+} \neq \Omega_{d-}$ or $\Omega_{p+} \neq \Omega_{p-}$, which implies the separation of the reflected LCP and RCP probe beams. In a narrow region around $\Omega_{d+} = \Omega_{d-}$ (Fig. 5a) and $\Omega_{p+} = \Omega_{p-}$ (Fig. 5b), the combination of ladder-EIT and three photon process in atomic medium lead to loss in both LCP and RCP probe beams, negative GH shifts of orthogonal circularly polarized beams are achieved owing to the superluminal propagation. In Fig. 5c and Fig. 5d, the separate distance ($[S_{GH}(R) - S_{GH}(L)]$) are plotted as a function of drive (Ω_{d-}) and probe (Ω_{p-}) field intensities. The values of $[S_{GH}(R) - S_{GH}(L)]$ are switched from negative to positive at the critical points $\Omega_{d+} = \Omega_{d-}$ (Fig. 5c) or $\Omega_{p+} = \Omega_{p-}$ (Fig. 5d). Moreover, for a certain value of Ω_{d+} (Ω_{p+}) in Fig. 5a (Fig. 5b), positive and negative GH shifts are simultaneously enhanced which further lead to increase the separate distances as shown in Fig. 5c and Fig. 5d, the maximal value can be reached to $272.7\mu\text{m}$ when the intensity of the applied fields are adjusted. Thus, the scheme could be employed as a tunable beam splitter for orthogonal circularly polarized light beams [56].

3.4 The Effect of Probe Field Frequency Detuning on the Separate Distance

The effect of probe field frequency detuning δ on the separate distance is also a significant issue to be considered. The values of $[S_{GH}(R) - S_{GH}(L)]$ versus the probe field frequency detuning δ with different drive and probe fields are shown in Fig. 6. As the probe field frequency detuning dramatically modified the susceptibilities of double ladder energy level system, the behavior of GH shifts are manipulated result from the modification of the resonant condition of the cavity [33], In Fig. 6a and Fig. 6b, nonzero separate distance could be achieved in the region $-10\gamma < \delta < 10\gamma$, since the difference between χ_- and χ_+ lead to different values of GH shifts for LCP and RCP probe beams.

As Fig. 6a and Fig. 6b shown, both LCP and RCP beams experience loss (as shown in Fig. 3–Fig. 4) in the region $|4\gamma| < \delta < |10\gamma|$, the GH shifts for both LCP and RCP beams are negative based on the above discussions, relatively small separate distance is obtained. While in the region $\delta < |4\gamma|$, both gain and loss are generated at the same time for LCP and RCP probe beams (as shown

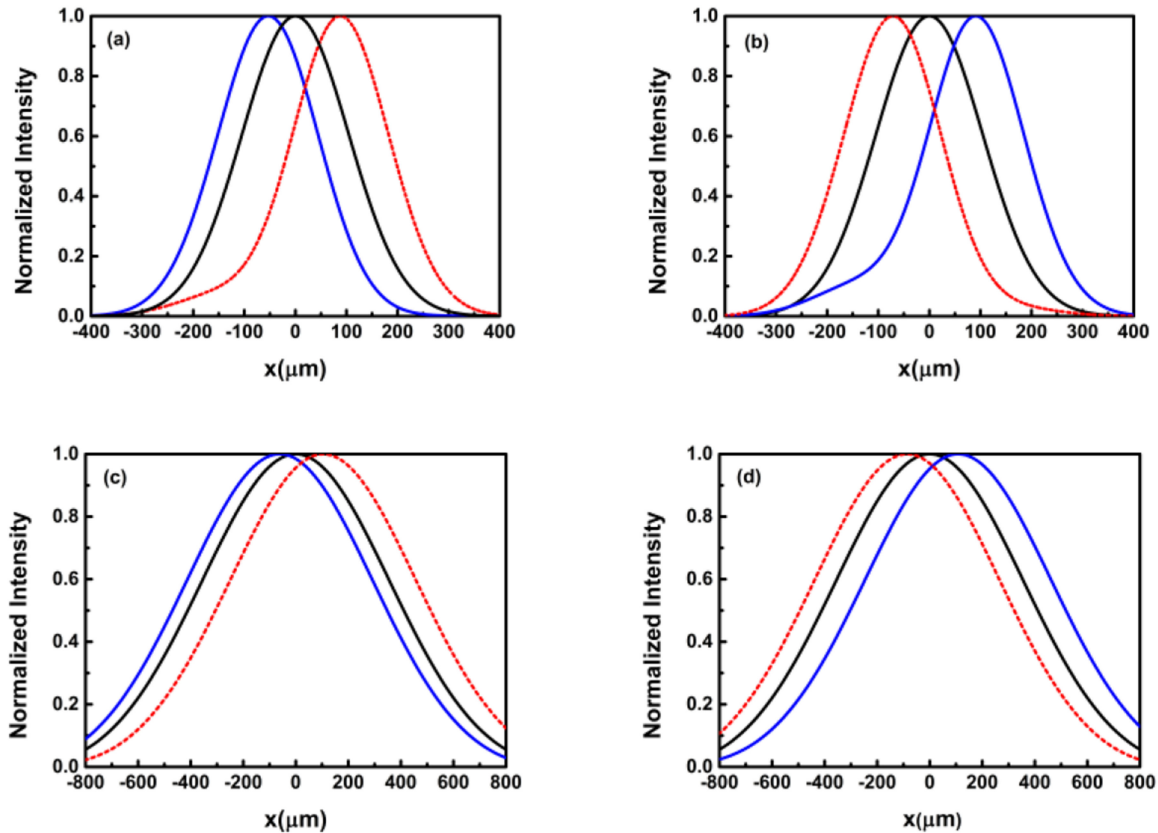


Fig. 7. Plot of normalized intensity profiles of incident linearly polarized light beam (black solid lines) and reflected LCP (red dashed lines) and RCP (blue solid lines) light beams. In all of the figures $\Omega_{p+} = \Omega_{p-} = 0.1\gamma$, $\Omega_{d+} = 5\gamma$, (a) $W = 100\lambda_p$, $\Omega_{d-} = 2.5\gamma$, (b) $W = 100\lambda_p$, $\Omega_{d-} = 7.5\gamma$, (c) $W = 500\lambda_p$, $\Omega_{d-} = 2.5\gamma$, (d) $W = 500\lambda_p$, $\Omega_{d-} = 7.5\gamma$, $\theta = 30^\circ$, the rest of parameters are the same as in Fig. 2.

in Fig. 3–Fig. 4). Subluminal and superluminal wave propagation are simultaneously realized which lead to opposite GH shifts for LCP and RCP probe beams. The separate distance is enhanced and the largest value can be reached to $320\mu\text{m}$ (absolute value) when the probe field detuning is adjusted ($\delta = -0.8\gamma$). Moreover, both drive and probe fields can be employed to further manipulate the separate distance.

3.5 Beam Simulation

In the above calculations and discussions, we have demonstrated tunable and simultaneously opposite GH shifts for reflected LCP and RCP probe beams based on stationary phase theory. In order to give an intuitive understanding and verify the theoretical analysis, numerical simulations are performed based on Eq. (10)–(13) following the Ref. [42], [53]. A well-collimated beam with spatial Gaussian profile is considered to incident on the cavity. The waist of the incident beam is $W = 100\lambda_p$ and $500\lambda_p$, the incident angle is fixed at $\theta = 30^\circ$. The normalized intensity profiles of the incident and reflected probe beams are shown in Fig. 7 for four cases (a) $W = 100\lambda_p$, $\Omega_{d-} = 2.5\gamma$, (b) $W = 100\lambda_p$, $\Omega_{d-} = 7.5\gamma$, (c) $W = 500\lambda_p$, $\Omega_{d-} = 2.5\gamma$, (d) $W = 500\lambda_p$, $\Omega_{d-} = 7.5\gamma$. The black solid lines refer to the incident beams (linearly polarized), whereas the red dashed and blue solid lines refer to the LCP and RCP probe beams respectively. It is shown in Fig. 7a–Fig. 7d that opposite GH shifts are simultaneously achieved for LCP and RCP probe beams. In Fig. 7a, the GH shift for LCP and RCP probe beam is positive and negative respectively with $\Omega_{d-} = 2.5\gamma$, while

the GH shift is switched from positive (negative) to negative (positive) for LCP (RCP) probe beams with $\Omega_d = 7.5\gamma$. The GH shifts are manipulated via only adjusting the drive field. For the case of $W = 500\lambda_p$, the result is still valid as shown in Fig. 7c and Fig. 7d. However, compared with the shape of the incident beam, the reflected probe beams are distorted owing to the effects of waist in Fig. 7a and Fig. 7b [33], [36], [57]. While in Fig. 7c and Fig. 7d, the shape of the reflected probe beams are nearly the same as the original shape of the incident Gaussian beam with a larger beam waist $W = 500\lambda_p$.

The above results have demonstrated the polarized beam splitting based on opposite GH shifts, related parameters were also used to control the separate distance. In experiment, the three photon based gain process and the cross talk effect between the two probe beams have been verified using cesium atomic vapor cell [50], [51]. The power of both probe and drive beams can be easily controlled by adjusting a half-wave plate before a polarizer, the polarization state are tuned employing the rotating polarizer and a quarter-wave plate [50], [51]. In addition, the double ladder energy level structure also can be realized in solid state systems (GaAs/AlGaAs quantum wells), the susceptibilities were easily controlled through the relative phase of the applied field and exciton spin relaxation, then the GH shifts are controlled [37].

4. Conclusions

In summary, we have theoretically investigated the behavior of the GH shifts for LCP and RCP probe beams reflected from the cavity containing double ladder energy level system. For symmetric case of the double ladder energy level system, the behavior of GH shifts for reflected LCP and RCP probe beams are identical. It is found that the LCP and RCP probe beams experiences opposite GH shifts at the same time, which is due to the realization of concurrently subluminal and superluminal propagation with asymmetric probe or drive fields cases. In addition, the behavior of the GH shifts for LCP and RCP probe beams are simultaneously manipulated by only adjusting the intensity of probe or drive fields. The dependence of the beam splitting on probe field detuning was discussed, the analysis demonstrated the parameters region to achieve a large separate distance (a maximal value of $320\ \mu\text{m}$ can be achieved). The configuration proposed in this paper has potential applications in tunable beam splitter for circularly polarized lights.

References

- [1] F. Goos and H. Hänchen, "Ein neuer und fundamentaler versuch zur totalreflexion," *Ann. Phys.*, vol. 436, no. 7/8, pp. 333–346, Dec. 1947.
- [2] K. Artmann, "Berechnung der seitenversetzung des totalreflektierten strahles," *Ann. Phys.*, vol. 437, no. 1, pp. 87–102, Jan. 1948.
- [3] R. H. Renard, "Total reflection: A new evaluation of the Goos–Hänchen shift," *J. Opt. Soc. Amer.*, vol. 54, no. 10, pp. 1190–1197, Oct. 1964.
- [4] T. Hashimoto and T. Yoshino, "Optical heterodyne sensor using the Goos–Hänchen shift," *Opt. Lett.*, vol. 14, no. 17, pp. 913–915, Sep. 1989.
- [5] Y. Wang, H. Li, Z. Cao, T. Yu, Q. Shen, and Y. He, "Oscillating wave sensor based on the Goos–Hänchen effect," *Appl. Phys. Lett.*, vol. 92, no. 6, pp. 61117-1–061117-3, Feb. 2008.
- [6] X. Wang *et al.*, "High-sensitivity temperature sensor using the ultrahigh order mode-enhanced Goos–Hänchen effect," *Opt. Exp.*, vol. 21, no. 11, pp. 13380–13385, May 2013.
- [7] C. W. Chen *et al.*, "Optical temperature sensing based on the Goos–Hänchen effect," *Appl. Opt.*, vol. 46, no. 22, pp. 5347–5351, Aug. 2007.
- [8] R. Briers, O. Leroy, and G. Shkerdin, "Bounded beam interaction with thin inclusions. Characterization by phase differences at Rayleigh angle incidence," *J. Acoustical Soc. Amer.*, vol. 108, no. 4, pp. 1622–1630, Jun. 2000.
- [9] X. Yin, L. Hesselink, Z. Liu, N. Fang, and X. Zhang, "Large positive and negative lateral optical beam displacements due to surface plasmon resonance," *Appl. Phys. Lett.*, vol. 85, no. 3, pp. 372–374, Jul. 2004.
- [10] Q. You, Y. Shan, S. Gan, Y. Zhao, X. Dai, and Y. Xiang, "Giant and controllable Goos–Hänchen shifts based on surface plasmon resonance with graphene-MoS₂ heterostructure," *Opt. Mater. Exp.*, vol. 8, no. 10, pp. 3036–3048, Oct. 2018.
- [11] V. K. Ignatovich, "Neutron reflection from condensed matter, the Goos–Hänchen effect and coherence," *Phys. Lett. A*, vol. 322, no. 1, pp. 36–46, Feb. 2004.
- [12] C. W. J. Beenakker, R. A. Sepkhanov, A. R. Akhmerov, and J. Tworzydło, "Quantum Goos–Hänchen effect in graphene," *Phys. Rev. Lett.*, vol. 102, no. 14, pp. 146804-1–146804-4, Apr. 2009.

- [13] V. O. Haan, J. Plomp, T. M. Rekveldt, W. H. Kraan, and A. A. van well, "Observation of the Goos-Hänchen shift with neutrons," *Phys. Rev. Lett.*, vol. 104, no. 1, pp. 010401-1–0104014, Jan. 2010.
- [14] J. S. Li, J. F. Wu, and L. Zhang, "Giant tunable Goos-Hänchen shifts based on prism/graphene structure in terahertz wave region," *IEEE Photon. J.*, vol. 6, no. 6, pp. 1–7, Dec. 2014.
- [15] Y. H. Wan, Z. Zheng, W. Kong, X. Zhao, and J. Liu, "Fiber-to-fiber optical switching based on gigantic Bloch-surface-wave-induced Goos-Hänchen shifts," *IEEE Photon. J.*, vol. 5, no. 1, pp. 1–7, Feb. 2013.
- [16] Y. Wang, Z. Cao, H. Li, J. Hao, T. Yu, and Q. Shen, "Electric control of spatial beam position based on the Goos-Hänchen effect," *Appl. Phys. Lett.*, vol. 93, no. 9, pp. 091103-1–091103-3, Sep. 2008.
- [17] L. Jiang, Q. Wang, Y. Xiang, X. Dai, and S. Wen, "Electrically tunable Goos-Hänchen shift of light beam reflected from a graphene-on-dielectric surface," *IEEE Photon. J.*, vol. 5, no. 3, pp. 1–8, Jun. 2013.
- [18] T. Tamir and H. L. Bertoni, "Lateral displacement of optical beams at multilayered and periodic structures," *J. Opt. Soc. Amer. A*, vol. 61, no. 10, pp. 1397–1413, Oct. 1971.
- [19] F. Schreier, M. Schmitz, and O. Bryngdahl, "Beam displacement at diffractive structures under resonance conditions," *Opt. Lett.*, vol. 23, no. 8, pp. 576–578, Apr. 1998.
- [20] C. Xu, J. Xu, G. Song, C. Zhu, Y. Yang, and G. S. Agarwal, "Enhanced displacements in reflected beams at hyperbolic metamaterials," *Opt. Exp.*, vol. 24, no. 19, pp. 21767–21776, Sep. 2016.
- [21] M. Tang *et al.*, "Narrow band optical filter using Goos-Hänchen shift in a cascaded waveguide structure," *Opt. Laser Technol.*, vol. 55, pp. 42–45, Feb. 2014.
- [22] T. Yu, H. Li, Z. Cao, Y. Wang, Q. Shen, and Y. He, "Oscillating wave displacement sensor using the enhanced Goos-Hänchen effect in a symmetrical metal-cladding optical waveguide," *Opt. Lett.*, vol. 33, no. 9, pp. 1001–1003, May 2008.
- [23] I. V. Shadrivov, A. A. Zharov, and Y. S. Kivshar, "Giant Goos-Hänchen effect at the reflection from left-handed metamaterials," *Appl. Phys. Lett.*, vol. 83, no. 13, pp. 2713–2715, Sep. 2003.
- [24] L. G. Wang and S. Y. Zhu, "Giant lateral shift of a light beam at the defect mode in one-dimensional photonic crystals," *Opt. Lett.*, vol. 31, no. 1, pp. 101–103, Jan. 2006.
- [25] I. V. Shoboleva, V. V. Moskalenko, and A. A. Fedyanin, "Giant Goos-Hänchen effect and fano resonance at photonic crystal surfaces," *Phys. Rev. Lett.*, vol. 108, no. 12, pp. 123901-1–123901-5, Mar. 2012.
- [26] H. M. Lai and S. W. Chan, "Large and negative Goos-Hänchen shift near the Brewster dip on reflection from weakly absorbing media," *Opt. Lett.*, vol. 27, no. 9, pp. 680–682, May 2002.
- [27] L. G. Wang, H. Chen, and S. Y. Zhu, "Large negative Goos-Hänchen shift from a weakly absorbing dielectric slab," *Opt. Lett.*, vol. 30, no. 21, pp. 2936–2938, Nov. 2005.
- [28] L. G. Wang and S. Y. Zhu, "Large positive and negative Goos-Hänchen shifts from a weakly absorbing left-handed slab," *J. Appl. Phys.*, vol. 98, no. 4, pp. 043522-1–043522-4, Aug. 2005.
- [29] M. Merano, A. Aiello, G. W. 't Hooft, M. P. van Exter, E. R. Eliel, and J. P. Woerdman, "Observation of Goos-Hänchen shifts in metallic reflection," *Opt. Lett.*, vol. 15, no. 24, pp. 15928–15934, Nov. 2007.
- [30] C. F. Li and Q. Wang, "Prediction of simultaneously large and opposite generalized Goos-Hänchen shifts for TE and TM light beams in an asymmetric double-prism configuration," *Phys. Rev. E*, vol. 69, no. 5, pp. 055601-1–055601-4, May 2004.
- [31] L. Chen, Y. Zhu, Y. Peng, and S. Zhuang, "Theoretical and experimental study of opposite lateral shifts and polarization beam splitting on symmetrical metal-cladding waveguides," *J. Opt.*, vol. 12, no. 7, pp. 1–6, Jun. 2010.
- [32] X. L. Hu, Y. D. Huang, W. Zhang, D. K. Qing, and J. D. Peng, "Opposite Goos-Hänchen shifts for transverse electric and transverse-magnetic beams at the interface associated with single-negative materials," *Opt. Lett.*, vol. 30, no. 8, pp. 899–901, Apr. 2005.
- [33] L. G. Wang, M. Ikram, and M. S. Zubairy, "Control of the Goos-Hänchen shift of a light beam via a coherent driving field," *Phys. Rev. A*, vol. 77, no. 2, pp. 023811-1–023811-5, Feb. 2008.
- [34] S. Q. Ziauddin and M. Suhail Zubairy, "Coherent control of the Goos-Hänchen shift," *Phys. Rev. A*, vol. 81, no. 2, pp. 023821-1–023821-9, Feb. 2010.
- [35] M. Abbas, Z. Uddin, and S. Qamar, "Amplitude control of the Goos-Hänchen shift via a Kerr nonlinearity," *Laser Phys. Lett.*, vol. 11, no. 1, pp. 1–8, Feb. 2014.
- [36] H. R. Hamed, A. Radmehr, and M. Sahr, "Manipulation of Goos-Hänchen shifts in the atomic configuration of mercury via interacting dark-state resonances," *Phys. Rev. A*, vol. 90, no. 5, pp. 053836-1–053836-11, Nov. 2014.
- [37] S. H. Asadpour, R. Nasehi, H. R. Soleimani, and M. Mahmoudi, "Phase control of Goos-Hänchen shift via biexciton coherence in a multiple quantum well," *Superlattices Microstruct.*, vol. 85, pp. 112–123, May 2015.
- [38] C. Y. Luo, X. Y. Dai, Y. J. Xiang, and S. C. Wen, "Enhanced and tunable Goos-Hänchen shift in a cavity containing colloidal ferrofluids," *IEEE Photon. J.*, vol. 7, no. 4, pp. 1–10, Aug. 2015.
- [39] W. X. Yang, S. Liu, Z. Zhu, Ziauddin, and R.-K. Lee, "Tunneling-induced giant Goos-Hänchen shift in quantum wells," *Opt. Lett.*, vol. 40, no. 13, pp. 3133–3136, Jun. 2015.
- [40] Ziauddin, Y.-L. Chuang, and R.-K. Lee, "Giant Goos-Hänchen shift using PT symmetry," *Phys. Rev. A*, vol. 92, no. 1, pp. 013815-1–013815-7, Jul. 2015.
- [41] S. P. Liu, W. X. Yang, and Z. H. Zhu, "Coherent control of the Goos-Hänchen shift via Fano interference," *J. Appl. Phys.*, vol. 119, no. 14, pp. 143101-1–143101-8, Apr. 2016.
- [42] S. Asiri, J. P. Xu, M. Al-Amri, and M. S. Zubairy, "Controlling the Goos-Hänchen and Imbert-Fedorov shifts via pump and driving fields," *Phys. Rev. A*, vol. 93, no. 1, pp. 013821-1–013821-6, Jan. 2016.
- [43] R. Nasehi, "Transverse magnetic field effect on the giant Goos-Hänchen shifts based on a degenerate two-level system," *Laser Phys. Lett.*, vol. 15, no. 6, pp. 1–11, Apr. 2018.
- [44] S. H. Asadpour, "Goos-Hänchen shifts due to spin-orbit coupling in the carbon nanotube quantum dot nanostructures," *Appl. Opt.*, vol. 56, no. 8, pp. 2201–2208, Mar. 2017.
- [45] S. H. Asadpour, H. R. Hamed, and M. Jafari, "Enhancement of Goos-Hänchen shift due to a Rydberg state," *Appl. Opt.*, vol. 57, no. 15, pp. 4013–4019, May 2018.
- [46] A. K. Patnaik, S. Roy, and J. R. Gord, "All-optically controlled concurrent slow-fast light pair," *Opt. Lett.*, vol. 36, no. 16, pp. 3272–3274, Aug. 2011.

- [47] O. Hosten and P. Kwiat, "Observation of the spin hall effect of light via weak measurements," *Science*, vol. 319, no. 5864, pp. 787–790, Feb. 2008.
- [48] T. T. Tang, L. Bi, L. Luo, J. Li, Y. F. Zhang, and P. Sun, "Magneto-optical imbert–fedorov effect in prism coupling configuration," *IEEE. Photon. J.*, vol. 9, no. 3, pp. 1–7, Jun. 2017.
- [49] X. J. Zhang, H. H. Wang, C. Z. Liu, G. W. Zhang, L. Wang, and J. H. Wu, "Controlling transverse shift of the reflected light via high refractive index with zero absorption," *Opt. Exp.*, vol. 25, no. 9, pp. 10335–10344, May 2017.
- [50] P. S. Hsu, A. K. Patnaik, and G. R. Welch, "Study of resonant $\chi(3)$ processes in a double-ladder system," *J. Modern Opt.*, vol. 55, pp. 3109–3119, Nov. 2008.
- [51] P. S. Hsu, G. R. Welch, J. R. Gord, and A. K. Patnaik, "Propagation dynamics of controlled cross-talk via interplay between $\chi(1)$ and $\chi(3)$ processes," *Phys. Rev. A*, vol. 83, no. 5, pp. 053819-1–053819-8, May 2011.
- [52] A. Ghosh and P. Fischer, "Chiral molecules split light: Reflection and refraction in a chiral liquid," *Phys. Rev. Lett.*, vol. 97, no. 17, pp. 173002-1–173002-4, Oct. 2006.
- [53] C. F. Li, "Unified theory for Goos-Hänchen and Imbert-Fedorov effects," *Phys. Rev. A*, vol. 76, no. 1, pp. 013811-1–013811-7, Jul. 2007.
- [54] A. Aiello, "Goos-Hänchen and Imbert-Fedorov shifts: A novel perspective," *New J. Phys.*, vol. 14, pp. 1–12, Jan. 2012.
- [55] D. A. Steck, Cesium D line data. Dec. 2010. [Online]. Available: <http://steck.us/alkalidata>
- [56] X. Chen, M. Shen, Z. F. Zhang, and C. F. Li, "Tunable lateral shift and polarization beam splitting of the transmitted light beam through electro-optic crystals," *J. Appl. Phys.*, vol. 104, no. 12, pp. 123101-1–123101-6, Dec. 2008.
- [57] S. Q. Ziauddin, "Control of the Goos-Hanthen shift using a duplicated two-level atomic medium," *Phys. Rev. A*, vol. 85, no. 5, pp. 055804-1–055804-5, May 2012.